**Article:**
Zhao, Z., Li, Y., Xu, R. et al. (2026) Intercomparison of methods for disentangling local and nonlocal biophysical impacts of land cover changes. Earth's Future, 14 (5). e2025EF007704. ISSN: 2328-4277

https://doi.org/10.1029/2025ef007704

Earth's Future

RESEARCH ARTICLE
10.1029/2025EF007704

# Intercomparison of Methods for Disentangling Local and Nonlocal Biophysical Impacts of Land Cover Changes

**Zijun Zhao[1,2], Yan Li[1,2], Ru Xu[3], Ronny Meier[4], Laibao Liu[5], Liang Chen[6], Lei Zhao[7,8], Yiqing Liu[1,2], Shuangshuang Zi[1,2], and Difei Zhao[1,2]**

[1]State Key Laboratory of Earth Surface Processes and Hazards Risk Governance (ESPHR), Faculty of Geographical Science, Beijing Normal University, Beijing, China, [2]Institute of Land Surface System and Sustainable Development, Faculty of Geographical Science, Beijing Normal University, Beijing, China, [3]Leverhulme Centre for Climate Change Mitigation, School of Biosciences, University of Sheffield, Sheffield, UK, [4]Umweltschutz, Stadt Luzern, Lucerne, Switzerland, [5]Department of Geography, Institute for Climate and Carbon Neutrality, The University of Hong Kong, Hong Kong, China, [6]Earth and Atmospheric Sciences, University of Nebraska–Lincoln, Bessey Hall, Lincoln, NE, USA, [7]Department of Civil and Environmental Engineering, University of Illinois at Urbana-Champaign, Urbana, IL, USA, [8]National Center for Supercomputing Applications, University of Illinois at Urbana-Champaign, Urbana, IL, USA

**Key Points:**

- Using unified deforestation experiments to compare methods for separating local and nonlocal biophysical effects of land cover change
- Methods agree on spatial and seasonal patterns of local and nonlocal effects, while regional differences reflect method assumptions
- Practical guidance is provided for each method under different research and data contexts

**Supporting Information:**

Supporting Information may be found in the online version of this article.

**Correspondence to:**

Y. Li,
yanli.geo@gmail.com

**Citation:**

Zhao, Z., Li, Y., Xu, R., Meier, R., Liu, L., Chen, L., et al. (2026). Intercomparison of methods for disentangling local and nonlocal biophysical impacts of land cover changes. *Earth's Future*, *14*, e2025EF007704. https://doi.org/10.1029/2025EF007704

Received 9 NOV 2025
Accepted 8 APR 2026

**Author Contributions:**

**Conceptualization:** Zijun Zhao, Yan Li
**Data curation:** Zijun Zhao, Difei Zhao
**Formal analysis:** Zijun Zhao, Yan Li
**Funding acquisition:** Yan Li
**Investigation:** Zijun Zhao, Yan Li
**Methodology:** Zijun Zhao, Yan Li
**Project administration:** Yan Li
**Resources:** Yan Li
**Software:** Zijun Zhao, Yan Li
**Supervision:** Yan Li
**Validation:** Zijun Zhao
**Visualization:** Zijun Zhao
**Writing – original draft:** Zijun Zhao
**Writing – review & editing:** Yan Li, Ru Xu, Ronny Meier, Laibao Liu, Liang Chen, Lei Zhao, Yiqing Liu, Shuangshuang Zi



**Abstract** The climatic impacts of land cover changes (LCCs) due to altered biophysical properties include local effects in LCC areas and nonlocal effects in both LCC and non-LCC areas resulting from atmospheric feedback. The biophysical impacts of LCC simulated by climate models typically represent only the total effects, that is, the sum of local and nonlocal effects. The respective local and nonlocal effects have been disentangled from climate model simulations using several methods. However, a systematic intercomparison of these methods under a comparable modeling framework is still lacking, hindering the complete understanding of LCC's biophysical effect on the methodological nature. This study employs a series of unified global deforestation experiments to assess the performance of existing methods in quantifying the local and nonlocal effects of LCC on land surface temperature. Results show that local effects derived by different methods exhibit overall consistent latitudinal and seasonal patterns compared to those in observational data sets, including the transition zone between warming and cooling across the Northern Hemisphere. The separated nonlocal effects, which dominate the total effects, can be reproduced with broad similarity across methods. Nevertheless, regional discrepancies exist, reflecting the different assumptions of each method. We further discuss and summarize the strengths and limitations of each approach and offer practical suggestions on their usage. This study provides methodological guidance for the quantitative assessment of biophysical climate effects of LCC across multi-scales for climate change research.

**Plain Language Summary** Changes in land cover, such as deforestation, influence the climate by altering how land absorbs sunlight, releases heat, and exchanges moisture with the atmosphere. These changes cause both local effects, in the regions where land cover changes occur, and nonlocal effects that spread through the atmosphere and affect other regions. Climate models are widely used to study these impacts, but they usually simulate only the combined effects of these two. Different methods exist to separate local and nonlocal effects. Until now, these methods have not been systematically compared, making it difficult to interpret their results. In this study, we use a set of global deforestation experiments to compare existing major methods for disentangling between local and nonlocal land surface temperature changes. We find the large-scale patterns of local and nonlocal effects are broadly consistent across methods, but regional differences remain due to each method's assumptions. Our results offer practical guidance on how to choose and apply these methods for different research objectives and data contexts.

## 1. Introduction

Human-induced land cover changes (LCCs), such as deforestation driven by agricultural expansion and urbanization, affected approximately 18%–29% of the ice-free lands (Hansen et al., 2010; Intergovernmental Panel On Climate Change, 2022; Luyssaert et al., 2014; Ramankutty & Foley, 1999; Schneider et al., 2009). LCCs influence climate through both biogeochemical (primarily related to the carbon cycle) and biophysical processes (radiative and non-radiative processes associated with albedo, evapotranspiration change, etc.) (Alkama & Cescatti, 2016; Amali et al., 2025; Bathiany et al., 2010; Boysen et al., 2014, 2020; Claussen et al., 2001; Kan

et al., 2025), resulting in climatic changes at local, regional, and even global scales (Cui & Graf, 2009; Devaraju et al., 2015; Li et al., 2023; Pitman et al., 2011).

Unlike biogeochemical effects, which operate globally in a relatively uniform way, biophysical impacts of LCC are more heterogeneous, affecting not only the climate in areas experiencing LCC but also other remote areas without LCCs (non-LCC areas), referred to as local and nonlocal effects, respectively (Winckler et al., 2017a), and their combination constitutes the total climate effects of LCC. Local effects are driven by changes in biophysical properties—such as albedo, evapotranspiration, aerodynamic resistance—which affect surface energy balance and fluxes without perturbing large-scale atmospheric conditions (Chen et al., 2024; Devaraju et al., 2018; Huang et al., 2020; Lee et al., 2011; Li et al., 2015). In contrast, nonlocal effects occur when LCC creates a sufficiently large perturbation to atmospheric circulation, which then propagates to influence climate in other LCC and non-LCC areas at regional and even global scales (Di Vittorio et al., 2018; Li et al., 2024; Portmann et al., 2022; Winckler, Lejeune, et al., 2019). Given the different scales and underlying processes, a separate consideration of local and nonlocal effects beyond their combined effects is crucial for understanding the multi-process, multi-scale climatic impacts of LCCs and for formulating effective land-based climate change mitigation and adaptation strategies (Pongratz et al., 2021).

Several approaches have been proposed to quantify the impact of LCCs on local and nonlocal land surface temperature using observations and climate model simulations. In observations, LCC effects are typically estimated by comparing climate variables at locations experiencing LCC versus regions experiencing no or a different degree of LCC at paired weather stations, eddy covariance sites (Lee et al., 2011; Yuan et al., 2021; Zhang et al., 2014), or in satellite data (Li et al., 2015). Although these observation-based space-for-time approaches primarily capture local effects while excluding large-scale nonlocal influences, they provide direct measures of LCC impacts at much finer spatial resolution (Duveiller et al., 2018a; Li et al., 2015; Prevedello et al., 2019). In contrast, typical numerical LCC experiments using climate model simulations capture the total climate response to LCCs but at much coarser spatial resolution. Additional methodologies are required to separate the signal into local and nonlocal effects (Boisier et al., 2012; Chalita & Le Treut, 1994; Jäger et al., 2026). One classical separation approach is to use land-only (i.e., offline) LCC simulations to quantify local effects without atmospheric feedback (Gibbard et al., 2005), and then obtain the nonlocal effects by subtracting them from the total effects from the land-atmosphere coupled LCC simulations. With the advent of climate models that provide subgrid-level outputs (e.g., at the Plant Function type (PFT) level), it has become possible to separate local and nonlocal effects through subgrid comparisons (Chen & Dirmeyer, 2020; Malyshev et al., 2015; Schultz et al., 2016). Another approach involves specially designed "checkerboard" LCC experiments (De Hertog et al., 2023; Winckler et al., 2017a), where the local and nonlocal effects are disentangled through spatial interpolation of model outputs. In addition, several postprocessing techniques have been successfully applied to separate local and nonlocal effects from existing LCC model simulation outputs, such as the Land Use Model Intercomparison Project (LUMIP) (Lawrence et al., 2016). These include the Intrinsic Biophysical Mechanism (IBPM) approach (Chen & Dirmeyer, 2016; Lee et al., 2011; S. Liu et al., 2023), space-for-time methods such as window-based spatial comparison (Kumar et al., 2013; Lejeune et al., 2017) and regression techniques (Lejeune et al., 2018), as well as the most recent spectral climate signal separation method (Jäger et al., 2025, 2026).

Although these approaches are theoretically capable of disentangling local and nonlocal effects in climate model simulations, a systematic evaluation and intercomparison of them is still lacking. Given their substantial differences in assumptions, it remains unclear how well each method performs against observational benchmarks and how effectively it compares to the others. These approaches are often employed in separate studies with their own model choices and LCC designs, making direct comparisons of their results challenging. To fill this gap, this study provides a comprehensive evaluation and intercomparison of existing major methods for separately quantifying local and nonlocal effects on land surface temperature (LST) using unified deforestation experiments with the Community Earth System Model (CESM) 2.1.2. We analyze the spatial and seasonal variations of the local and nonlocal effects separated by different methods, assess their consistency, and discuss the strengths and limitations of each method. This study aims to evaluate the applicability and limitations of various methods within a uniform, comparable framework, providing methodological guidance for quantitative assessments of biophysical climate effects of LCC across multiple scales.

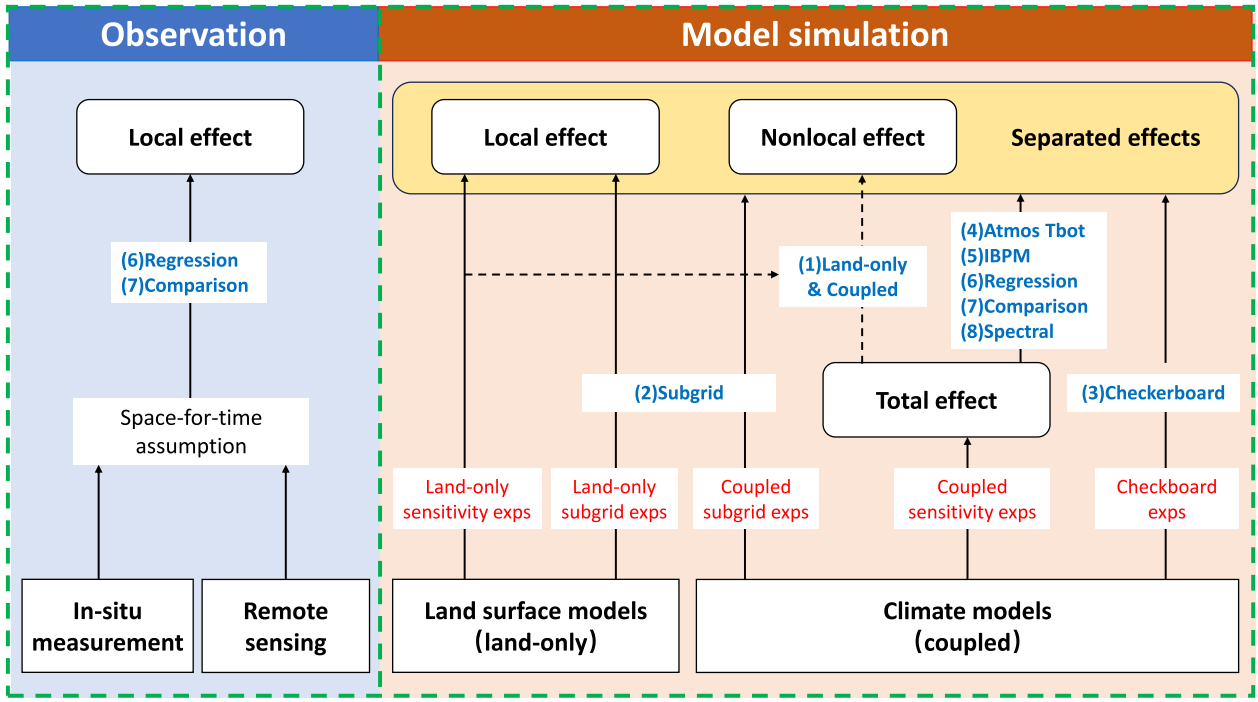


**Figure 1.** Overview of methods for quantifying local and nonlocal effects of land cover change based on observations and model simulations. Observational approaches (left) utilize in situ measurements and remote sensing data, combined with separation methods, to estimate local effects. Model simulation approaches rely on a suite of land-only and coupled simulation experiments. Local and nonlocal effects are obtained indirectly or directly through methods.

## 2. Data and Methods

### 2.1. Experimental Design

Figure 1 summarizes various approaches from the literature that separately quantify the local and nonlocal effects of LCC on climate (i.e., surface temperature response) using observational data and climate model simulations. To compare these approaches, we conducted a series of coupled and land-only LCC sensitivity experiments (a control run and another with deforestation) using CESM 2.1.2 (Danabasoglu et al., 2020) and its land component, the Community Land Model 5.0 (CLM5) (Lawrence et al., 2019). For coupled simulations, we used the component set F2000climo, which couples the land and atmosphere, to conduct the control (CTL) and deforestation (DEF) experiments. For land-only simulations, we used the component set I2000Clm50Sp for the CTL and DEF experiments, with no feedback to the atmosphere. Both model components are configured with fixed atmospheric $CO_2$ concentrations and prescribed sea surface temperature and sea ice conditions. The I2000Clm50Sp configuration includes prescribed satellite phenology and is driven by cycling GSWP forcing of the year 2000. The model grids of all simulations were set to 1.875° × 2.5° (F19_G16), and each simulation was run for 35 years with monthly output. At this resolution, local effects should be interpreted as "local" relative to the grid cell size, neglecting their landscape-scale variations and possible nonlocal effects triggered by LCC within the grid, especially when the grid cell size is large. The first 5 years were used as spin-up, and the last 30 years were for analysis. All analyses were restricted to the region between 60°S and 80°N to ensure spatial comparability across all methods. The land surface temperature we analyzed is defined as a radiative surface temperature consistent with remote sensing products (Duveiller et al., 2018a; Li et al., 2015), and is computed from the emitted longwave radiation using the Stefan–Boltzmann law, assuming an emissivity of 1.

Several deforestation scenarios were designed based on the year 2000 land cover in CTL by converting trees and shrubs (PFTs 1–11) to grasslands (PFTs 12–14) in proportion to the existing grassland PFTs composition (Figure S1a in Supporting Information S1). Note that the designed global deforestation scenarios represent an idealized LCC scenario for method-comparison purposes; the real-world LCC would not occur at this massive scale. Below is a summary of the four land cover scenarios used in this study, which were implemented in both land-only and coupled simulations, as described in Table 1.

**Table 1**
*Land Cover Scenarios and Experiments in This Study*

| Land cover scenario | Description | Experiments |
|---|---|---|
| Control (CTL) | Default year 2000 land cover | Exp1: Land-only CTL<br>Exp2: Coupled CTL |
| Deforestation (DEF) | Full deforestation in every grid cell | Exp3: Land-only DEF<br>Exp4: Coupled DEF |
| Deforestation_min (DEF_min) | 0.01% forest and shrub retained in every deforestation grid cell | Exp5: Land-only DEF_min<br>Exp6: Coupled DEF_min |
| Checkerboard | Full deforestation in alternating grid cells | Exp7: Coupled checkerboard |

1. CTL: The default year 2000 land cover map for the control experiments.
2. DEF: All forest and shrub PFTs (PFT 1–11) were converted to grassland PFTs (PFT 12–14), representing a global complete deforestation.
3. DEF_min: Similar to DEF, except forest and shrub PFTs were retained in a minimal non-zero fractional area (0.01%) instead of zero (Chen & Dirmeyer, 2020). This ensures consistency with the complete deforestation scenario regarding climate impacts while allowing subgrid outputs of forest and shrub PFTs.
4. DEF_checkerboard: A checkerboard deforestation scenario, where forest and shrub PFTs in every other grid cell were converted to grassland along latitude and longitude (Figure S1b in Supporting Information S1). The total area of deforestation is about half of the DEF scenario.

### 2.2. Methods of Quantifying Local and Nonlocal Effects

The above-described set of experiments enables us to apply different methods to separate local and nonlocal effects of LCC and compare their results (Table 2).

#### 2.2.1. Land-Only and Coupled Simulation Method

Local and nonlocal effects of LCC can be quantified by comparing the climate sensitivity to LCC in land-only simulations to that in coupled simulations. In the land-only simulations, the land surface model is driven by prescribed atmospheric forcing (i.e., land and atmosphere are not coupled). Therefore, the differences between the CTL and the DEF experiments from land-only simulations correspond to the local effects of deforestation ($\Delta T_{\text{local}}$) without any feedback from the atmosphere.

In contrast, for typical climate models in which the land and atmosphere components are coupled, the differences between the CTL and DEF experiments reflect the total effects, combining local effects and nonlocal effects induced by atmospheric feedback (i.e., changes in atmospheric states). The nonlocal effects ($\Delta T_{\text{nonlocal}}$) can be obtained by subtracting the local effects from the total effects of the coupled simulation.

#### 2.2.2. Subgrid Method

Some models represent land heterogeneity within a model grid cell through a nested hierarchy of PFTs at the subgrid level. Taking CLM5 as an example, all PFTs within each grid cell are driven by the same atmospheric forcing, and their surface energy balance and radiative fluxes are computed separately for each PFT but share the same soil moisture and soil temperature at the column level (a separate soil column modification was proposed by Schultz et al., 2016). Even though subsurface PFT states are not fully independent, the differences between PFTs are still primarily attributed to their distinct biophysical properties (e.g., forest vs. grass), reflecting local effects. This subgrid method allows local effects to be quantified from either land-only or coupled simulations. However, its interpretation remains dependent on the model's representation of subgrid processes (Meier et al., 2018; Schultz et al., 2016).

As the subgrid PFT differences imply a conversion from 100% forest and shrub to 100% grassland (each PFT is 100% pure), they should be multiplied by the LCC fraction (i.e., the fraction of forest PFT removed) in the grid cell to obtain local effects (Equation 1). The subgrid differences within the same grid cell for the same PFT between the CTL and DEF coupled experiments give nonlocal effects (Equation 2), reflecting the climatic changes induced by atmospheric feedbacks from deforestation. Nonlocal effects cannot be directly obtained from

Earth's Future

10.1029/2025EF007704

**Table 2**
*Different Methods With Their Required Experiments and Key Assumptions to Quantify the Local and Nonlocal Effects of LCCs*

| Methods | Experiments | Key assumptions | Local effects | Nonlocal effects |
|---|---|---|---|---|
| (1) Land-only and Coupled | Exp1–4 | Changes in land-only simulation reflect local effects | Changes in land-only Exps | Residual between total effects (from coupled simulation) and local effects |
| (2) Subgrid | Land-only: Exp2, Exp4, Exp5<br>Coupled: Exp2, Exp6 | Subgrid differences reflect local effects | PFT difference between forest and nonforest, multiplied by LCC fraction | Changes in nonforest PFT between Exps |
| (3) Checkerboard | Exp2, Exp7 | Effects can be reconstructed by interpolation | Changes in LCC grids minus nonlocal effects, then interpolate | Interpolated changes in non-LCC grids |
| (4) Atmospheric Tbot | Exp2, Exp4 | Changes in Tbot represent atmospheric feedback | Residual between total effects (from coupled simulation) and nonlocal effects | Changes in the bottom layer of atmospheric air temperature |
| (5) IBPM | | Changes induced by biophysical factors under an unaffected atmospheric state | Calculated from biophysical contribution terms | Residual between total effects (from coupled simulation) and local effects |
| (6) Window Regression | | Space-for-time assumption | Regression sensitivity to LCC multiply LCC fraction | |
| (7) Spatial Comparison | | | Mean difference between LCC and non-LCC grids | |
| (8) Spectral Separation | | Spectral decomposition and reconstruction | Large-scale signals represented by low-degree spherical harmonics | Small-scale signals represented by high-degree spherical harmonics |

land-only simulations because atmospheric feedbacks are not included. Alternatively, they can be inferred by subtracting the land-only-derived local effects from the total effects from coupled simulations, similar to the residual approach adopted by the Land-only and Coupled method:

$$\Delta T_{\text{local}} = \left(T_{\text{DEF}}^{\text{forest}} - T_{\text{DEF}}^{\text{grass}}\right) \times \text{frac}^{\text{DEF}} \quad (1)$$

$$\Delta T_{\text{nonlocal}} = T_{\text{DEF}}^{\text{grass}} - T_{\text{CTL}}^{\text{grass}} \quad (2)$$

where $T_{\text{DEF}}^{\text{forest}}, T_{\text{DEF}}^{\text{grass}}, T_{\text{CTL}}^{\text{grass}}$ represent the PFT area weighted mean of subgrid-level LST of forest and grass PFTs in the deforestation experiment, and grass PFTs in the control experiment. $\text{frac}^{\text{DEF}}$ denotes the forest PFT fraction removed in the deforestation scenario.

### 2.2.3. Checkerboard Method

The Checkerboard method, introduced by Winckler et al. (2017a), imposes land cover changes in an alternating grid pattern (modifying one out of every $N$ grid cells, where $N = 2$ in our setup) in coupled simulations. Compared with the 100% deforestation scenario, where all forest and shrub PFTs are converted to grass, the checkerboard implementation allows the coexistence of LCC and adjacent non-LCC grid cells. LCC grid cells are influenced by both local and nonlocal effects, while adjacent non-LCC grid cells are only influenced by nonlocal effects. Therefore, the nonlocal effects can be estimated by spatially interpolating (e.g., bilinear) target variables from non-LCC grid cells across the entire domain. By subtracting the interpolated nonlocal effects from the climate changes of LCC grid cells, the local effects are isolated and can be interpolated to the entire domain.

### 2.2.4. Atmospheric Tbot Method

Changes in atmospheric air temperature in the deforestation experiment are triggered by atmospheric feedback and thus, by definition, represent the nonlocal effects of LCC. We used changes in the bottom layer of atmospheric air temperature ($T_{\text{bottom}}$) to approximate nonlocal effects on LST, assuming similar responses between $T_{\text{bottom}}$ and LST to LCCs (Figure S2a in Supporting Information S1, $R^2 = 0.938$, RMSE = 0.185 K, $\lambda = 0.946$). The local effect is then obtained by subtracting the nonlocal effects from the total effects. Accordingly, this separation method is referred to as the Atmospheric Tbot method.

### 2.2.5. Intrinsic Biophysical Mechanism (IBPM) Method

The IBPM method, derived from surface energy balance equations, decomposes LCC-induced LST changes into individual biophysical factors, including surface albedo, aerodynamic resistance, and the Bowen ratio (Lee et al., 2011). The IBPM assumes that local perturbations by small-scale land cover changes are insufficient to trigger atmospheric changes; therefore, the calculated LST changes approximate the local effects of LCCs (Equation 3):

$$\Delta T_{\text{local}} \approx \frac{\lambda_0}{1+f}(\Delta R_n) + \frac{-\lambda_0}{(1+f)^2}(R_n)\left(\Delta f_1 + \Delta f_2\right) \quad (3)$$

where $R_n$ represents the net surface radiation, $\lambda_0$ is the local climate sensitivity ($\lambda_0 = \frac{1}{4\sigma T_a^3}$), and $f$ is the energy redistribution factor, where $f_1$ and $f_2$ represent contributions from changes in aerodynamic resistance and the Bowen ratio, respectively. Further details on the IBPM derivation are provided in Text S1 in Supporting Information S1. These variables without $\Delta$ are derived from the coupled CTL experiment (Exp2), and $\Delta$ variables denote the difference between the coupled DEF (Exp4) and CTL experiments (Exp2). As an approximate solution, the calculated LST may include outliers (due to $\Delta f_1$ and $\Delta f_2$ terms), which were subsequently filtered by restricting the valid value range to the 0.01%–99.9% percentile of the simulated total effects across the entire domain. Nonlocal effects from atmospheric feedback can be obtained by subtracting local effects from total effects.

#### 2.2.6. Window Regression Method

With the space-for-time assumption, LCC acts as a spatially heterogeneous local forcing that influences the climate of each grid cell, while other nonlocal climatic forcings (e.g., greenhouse gases) exert relatively uniform effects across neighboring cells. To extract the LCC impact, a moving window is employed to estimate the local temperature sensitivity to LCC by utilizing leveraging spatial variation in climate variables across grid cells within the window and their associated LCCs. Lejeune et al. (2018) proposed a multiple linear regression model to decompose the total effects into contributions from potential relevant explanatory factors (Equation 4): LCC fraction ($\mathrm{frac}^{\mathrm{DEF}}$), elevation (elev, resampled from the ETOPO1 topographic data set), latitude (lat), and longitude (lon).

$$\Delta T_{\mathrm{total}} = \beta_0 + \beta_1 \times \mathrm{frac}^{\mathrm{DEF}} + \beta_2 \times \mathrm{elev} + \beta_3 \times \mathrm{lat} + \beta_4 \times \mathrm{lon} \tag{4}$$

The LCC fraction term is related to the local effects, while the remaining terms are related to the nonlocal effects. We applied this model to the total effects derived from the coupled CTL (Exp2) and DEF experiments (Exp4). The regression coefficient, $\beta_1$, represents the local temperature sensitivity to LCC, which can be multiplied by the LCC fraction to yield the local effects (Equation 5). The nonlocal effects are represented by the sum of the remaining terms (the influence of regression residuals is negligible and thus not further discussed).

$$\Delta T_{\mathrm{local}} = \beta_1 \times \mathrm{frac}^{\mathrm{DEF}} \tag{5}$$

#### 2.2.7. Spatial Comparison Method

The space-for-time assumption can also be applied through spatial comparisons between LCC and non-LCC grids within a moving window, similar to methods used in observational studies (Li et al., 2015). In this framework, LCC grids whose climate is strongly influenced by LCC are compared with reference non-LCC grids or those with low LCC fractions. LCC and non-LCC grids are defined based on a specific LCC threshold and selection criteria. Based on the coupled CTL (Exp2) and DEF (Exp4) experiments, we followed Kumar et al. (2013) and set a threshold of 30% to distinguish between LCC (≥30%) and non-LCC (<30%) grids. We also adopted the sample selection strategy of Lejeune et al. (2017), in which a window is considered valid only if it contains at least 8 valid grid cells, including at least 3 high-LCC and 3 low-LCC grids. To satisfy this criterion, the window size is adaptively expanded—from an initial 5 × 5 to 7 × 7, 7 × 9, 9 × 9, and up to 11 × 11—until the requirements are met. The local effects are then estimated as the mean LST differences of LCC grids ($\overline{T_{\mathrm{forest}}}$) and non-LCC grids ($\overline{T_{\mathrm{grass}}}$) (Equation 6):

$$\Delta T_{\mathrm{local}} = \overline{T_{\mathrm{forest}}} - \overline{T_{\mathrm{grass}}} \tag{6}$$

Nonlocal effects are derived by subtracting local effects from total effects. The separated effects are assigned to the central grid of the window.

#### 2.2.8. Spectral Separation Method

This method separates local and nonlocal effects by spectral decomposition of LCC forcing and climate responses into a sum of cross-scale signals with different wavelengths based on spherical harmonics (Jäger et al., 2025, 2026). Large-scale components, represented by low-degree spherical harmonics, are interpreted as nonlocal effects associated with atmospheric adjustment and remote feedbacks, whereas small-scale components, represented by high-degree spherical harmonics, correspond to local effects driven by LCC forcing. The two effects are obtained by applying a spectral cutoff and reconstructing the corresponding spectral components.

In this study, we implemented this method using SCISSOR (Spectral ClImate Signal SeparatOR) developed by Jäger et al. (2025), a spherical harmonic–based signal separation framework that formalizes spectral decomposition via two modulation rules (MR1 and MR2). MR1 assigns the full amplitude of a spectral mode to nonlocal effects when the response spectrum exceeds the forcing spectrum, whereas MR2 applies a continuous weighting based on their relative magnitudes. We adopted MR2 to allow a smooth transition between local and nonlocal contributions across spatial scales. For mathematical derivation and more details of this method, please refer to Jäger et al. (2025).

### 2.3. Observational Benchmark for Local Effects

To evaluate the local effects of different methods, we compared them with two MODIS-based data sets of the potential biophysical impacts of deforestation on LST (Duveiller et al., 2018a; Li et al., 2015). The Li2015 data set employs a spatial comparison approach to estimate LST differences between forests and nearby open lands, reflecting the local effects of deforestation. The Duveiller2018 data set is constructed using a window regression framework and represents potential LST changes due to land conversion, specifically extracting LST changes from transitions from the broad forest category to other land cover types. To reconcile the different spatial resolutions with the model simulations, the benchmark data sets were resampled to the model resolution using linear interpolation. Since these benchmarks represent potential effects of complete deforestation, the resampled daily-averaged local effects were multiplied by the LCC fraction (Figure S1a in Supporting Information S1) for comparison with the simulated local effects.

### 2.4. Metrics for Assessing the Consistency of Different Methods

We evaluated the separated local and nonlocal effects across different methods by their sign consistency and a symmetric index of agreement ($\lambda$) (Duveiller et al., 2016). For sign consistency, we count the number of signs that agree with the majority sign across all methods at each grid.

The λ index is designed to meet the key requirements for quantifying the linear correlation and magnitude similarity between two data sets, as an extension of the Pearson correlation coefficient. Mathematically, for data sets $X$ and $Y$, λ is defined as:

$$\lambda = 1 - \frac{\sum_{i=1}^{n}(X_i - Y_i)^2}{\sum_{i=1}^{n}\left(X_i - \overline{X}\right)^2 + \sum_{i=1}^{n}\left(Y_i - \overline{Y}\right)^2 + n\left(\overline{X} - \overline{Y}\right)^2 + \kappa} \tag{7}$$

where

$$\kappa = \begin{cases} 2\left|\sum_{i=1}^{n}\left(X_i - \overline{X}\right)\left(Y_i - \overline{Y}\right)\right|, & r < 0 \\ 0, & r \geq 0 \end{cases} \tag{8}$$

and $r$ is the Pearson correlation. The symmetric index of agreement ($\lambda$) is a dimensionless metric ranging from 0 to 1. λ equals 1 when $X$ and $Y$ are identical in both amplitude and variability, and λ is 0 when $X$ and $Y$ are completely inconsistent or exhibit strong negative correlation. Therefore, λ provides an integrated measure of overall consistency that jointly reflects agreement in both trend and magnitude between the two data sets.

## 3. Results

### 3.1. Comparison of Separated Local Effects

The total effects of global deforestation, obtained from coupled control (CTL) and deforestation (DEF) experiments (Exp2 and Exp4), provide a foundation for separating local and nonlocal effects. The total effects showed a global cooling of −0.323 K (Figure S3 in Supporting Information S1), with year-round warming in the low latitudes and widespread cooling in the mid- and high-latitudes (except for winter warming). These simulated LST changes are consistent with previous studies (Chen & Dirmeyer, 2020; Devaraju et al., 2018; S. Liu et al., 2023; Luo et al., 2024) and can be used in the following analyses.

Figure 2 shows the spatial distribution of annual mean local effects of global deforestation on LST produced by different separation methods, ranging from −0.100 K (Spectral Separation) to +0.227 K (IBPM) over the deforested area. The overall pattern was warming in most low- and mid-latitudes and cooling in the northern high-latitudes, southern Africa, and western Australia. These spatial and latitudinal patterns also generally fell within the range of observational benchmarks from Li2015 and Duveiller2018 data sets. However, there were spatial coverage and regional inconsistencies (e.g., north of 60°N) between the two observational data sets. These inconsistencies are likely due to the methodological differences between spatial comparison and window regression

10.1029/2025EF007704

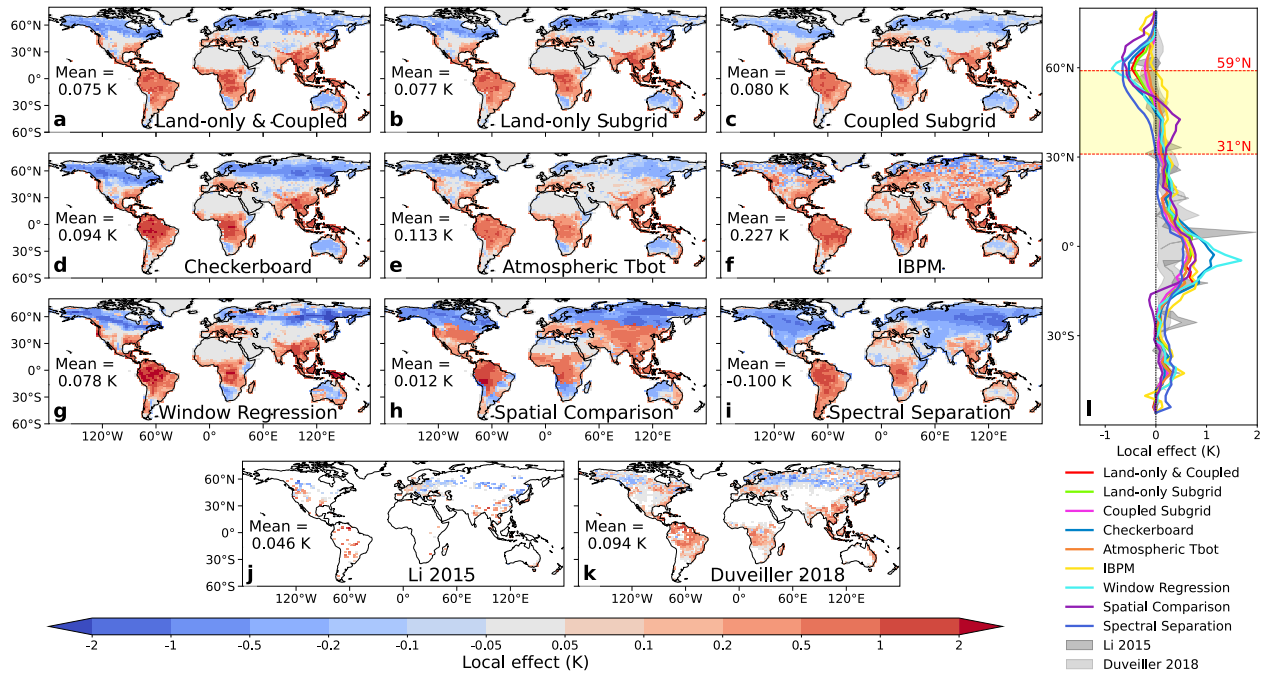


**Figure 2.** Spatial distribution of the separated local effects of deforestation on LST. Panels (a–i) show the annual mean local effects simulated by different separation methods, and panels (j–k) present satellite-based estimates from the Li2015 and Duveiller2018 data sets. The simulated local effects in the non-LCC areas are masked out. Panel (l) illustrates the latitudinal variations of annual mean local effects across methods and observational benchmarks, with yellow-shaded regions indicating divergent transitional zones between warming and cooling in the Northern Hemisphere. The gray shading indicates the 20%–80% zonal range from the Li2015 and Duveiller2018 data sets.

techniques, as similar inconsistencies arise when these two methods are applied to simulation experiments (Figures 2g and 2h).

Despite overall similarity, the simulated local effects showed notable regional discrepancies across methods. For example, all methods exhibited a clear transition from low-latitude warming to high-latitude cooling in the Northern Hemisphere, with the transition occurring at different latitudes. The transitional latitudes lie roughly between 31°N (Spectral Separation) and 59°N (IBPM) across different methods, suggesting varying strengths and spatial extents of local warming (Figure 2l), consistent with the wide range of latitudes for zero net local biophysical effect (30°N–56°N) reported in the literature (Lawrence et al., 2022). The Checkerboard, Window Regression, and Spatial Comparison produced the maximum warming exceeding 2 K in the tropical regions of the Amazon Basin, Congo Basin, and Maritime Continent (Figures 2d, 2g, and 2h). The IBPM indicated a more widespread warming than other methods, including regions with low forest fraction (western Asia and the Sahara) and high-latitude regions (Figure 2f). In contrast, Spectral Separation showed pronounced cooling over North America and central Asia, highlighting stronger local cooling effects in these regions (Figure 2i). The differences among methods became more pronounced at high latitudes, including stronger cooling with the Land-only Subgrid than the Coupled Subgrid, but prominent warming with the IBPM, and scattered warming with the Window Regression.

The seasonal variations of local effects also agreed well with the observational benchmarks (Figure 3). In the 30°S–30°N region, all methods consistently indicated persistent warming throughout the year with weak seasonality. Beyond this range, although warming remained evident in the summer, a cooling emerged in the winter months, gradually intensifying with increasing latitude and eventually leading to an annual cooling at higher latitudes. This pattern also indicated that seasonal warming still occurred during the summer months, despite the annual mean cooling observed in high-latitude regions.

Differences existed in the timing and magnitude of local effects, as well as in their seasonal variations, across methods. The maximum cooling was generally observed around 60°N between February and April. Such cooling was relatively weak in the Coupled Subgrid and the Atmospheric Tbot (Figure 3e, $>-1$ K), but rather strong in the

10.1029/2025EF007704

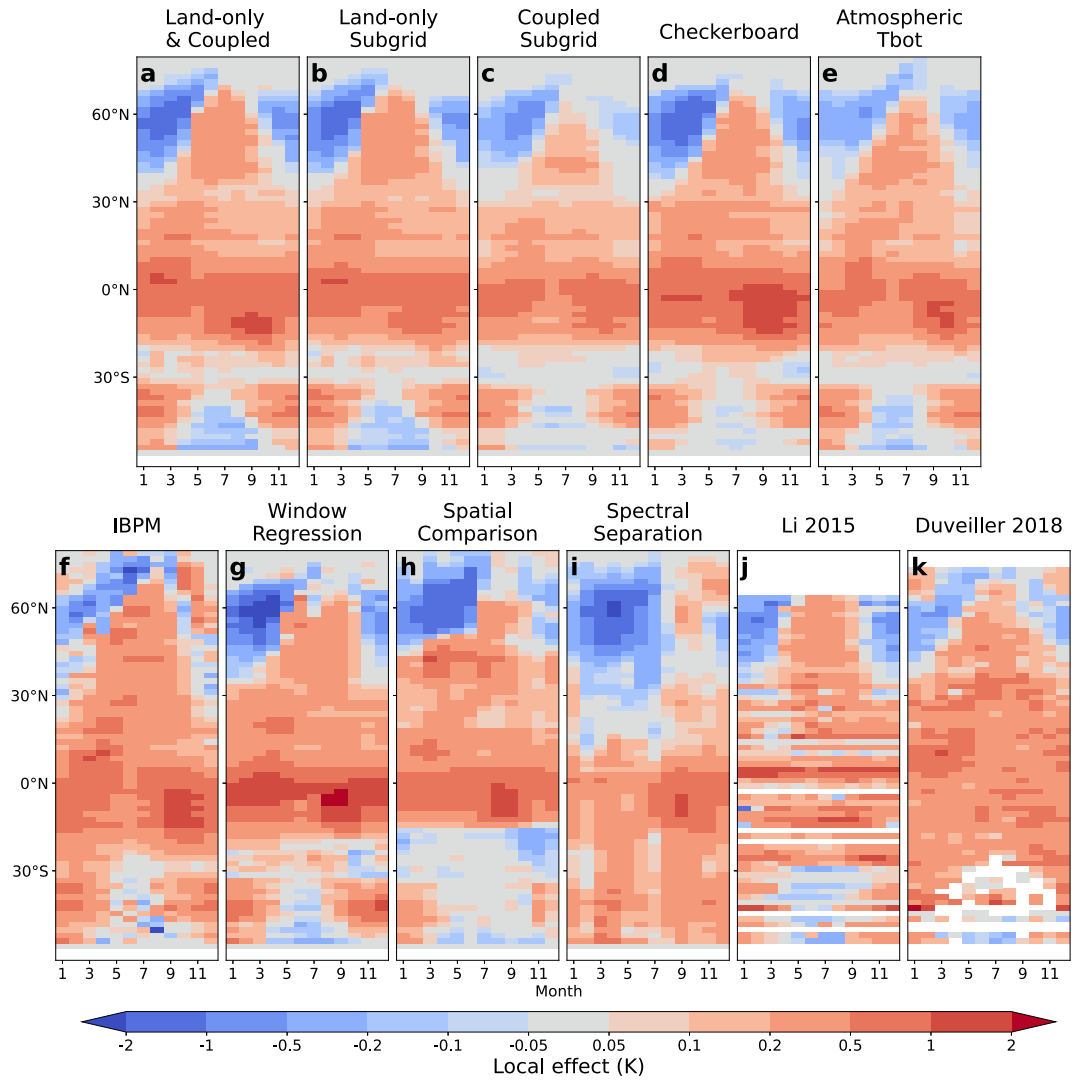


**Figure 3.** Seasonal and latitudinal variations of local effects from different methods (a–i) and observational data sets (j, k).

Window Regression (Figure 3g, <−2 K). In contrast, the maximum cooling identified by IBPM appeared northward around 70°N between April and July. Notably, IBPM and Spectral Separation were the few methods that captured a warming signal during the boreal winter (Figures 3f and 3i), in line with the observed data set (Figure 3k), although the associated spatial patterns differed (Figures 2f and 2i–2k). The maximum warming was typically observed near the equator between August and October. The Checkerboard and Window Regression detected the strongest warming, exceeding 2 K (Figures 3d and 3g), while the other methods found weaker responses (1–2 K). Spectral Separation exhibited weak but persistent cooling in the Northern Hemisphere and year-round warming in the Southern Hemisphere (Figure 3i). Due to limited and differing spatial coverage, observational data sets exhibited inconsistent seasonality, which compromises comparisons of timing and magnitude with model simulations.

### 3.2. Comparison of Separated Nonlocal Effects

The nonlocal effects exhibited an annual mean land cooling ranging from −0.421 K (Atmospheric Tbot) to −0.233 K (Checkerboard) across methods. In terms of magnitude, the nonlocal effects were much larger than the local effects (−0.100 K to +0.227 K), thereby dominating the total effects. Spatially, nonlocal effects manifested as cooling over mid- to high latitudes and warming over low latitudes, with regional features of cooling in Australia and southern Africa, and warming in parts of Europe. Unlike local effects, which had similar

10.1029/2025EF007704

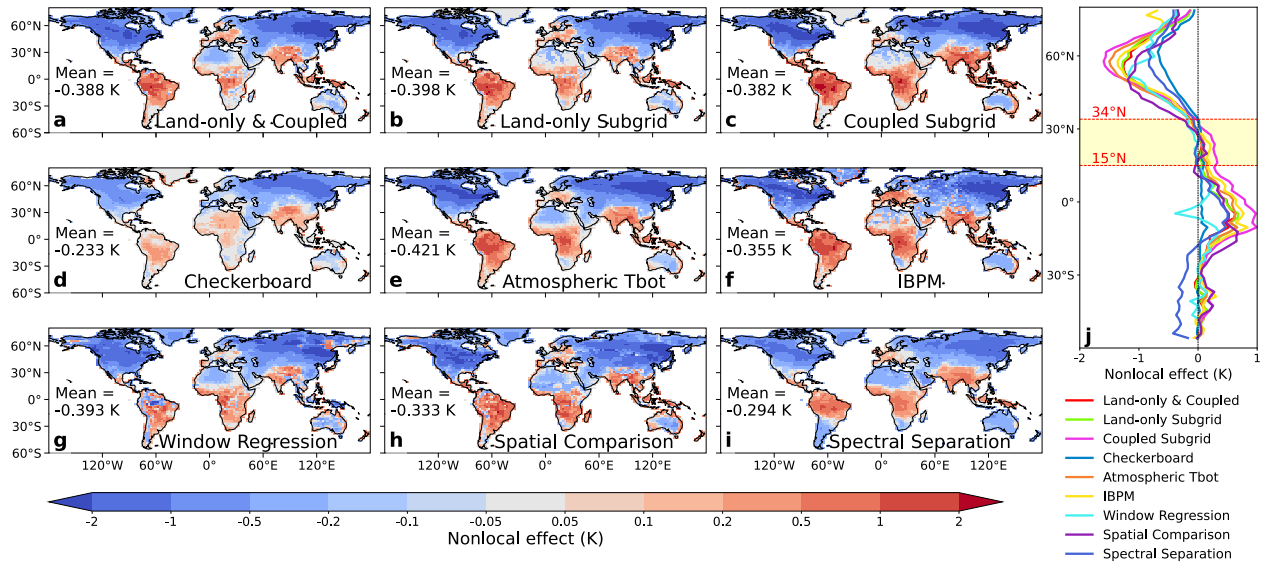


**Figure 4.** Spatial pattern of nonlocal effects of deforestation. Panels (a–i) display the annual mean nonlocal effects obtained from different separation methods. Panel (j) illustrates the latitudinal variation in annual mean nonlocal effects across methods, with yellow-shaded regions indicating divergent transitional zones between warming and cooling in the Northern Hemisphere.

magnitudes in low- and northern high-latitude regions, nonlocal effects exhibited stronger cooling in the northern high latitudes than warming in the tropics. Such zonal and regional differences are broadly consistent with previous findings for near-surface air temperature responses to LCC (Chen et al., 2026). Compared with local effects, nonlocal effects consistently dominated total effects across methods, accounting for 55%–85% of LCC grid cells and magnitudes 1.2–6.7 times larger than those of local effects (Table S1 in Supporting Information S1), particularly in regions with few LCCs.

A similar transition zone between warming and cooling was observed for nonlocal effects, but at a lower latitude than for local effects, spanning approximately 15°N (Window Regression) to 34°N (Checkerboard) (Figure 4j). Among all methods, the Checkerboard yielded the weakest nonlocal effects (Figure 4d, −0.233 K), with a distinct warming in the Sahara and Greenland that was not found in other methods. This is because the implemented deforestation was only half that in other experiments, and there were greater spatial extrapolation biases at locations far from the deforestation (Figure S1b in Supporting Information S1). In contrast, the Atmospheric Tbot produced the most substantial nonlocal effects (Figure 4e, −0.421 K), characterized by extensive cooling exceeding 2 K across large portions of 30°N–60°N and limited warming in tropical areas. The IBPM, Window Regression, and Spatial Comparison generated a few scattered cooling outliers over central Amazonia and warming in high-latitude regions.

The seasonality of nonlocal effects broadly resembled that of local effects but exhibited greater variations. A similar year-round nonlocal warming was confined to the narrower tropical region between 15°S and 10°N, with larger effects (≥1 K) from August to October. The regions spanning 55°S–15°S and 10°N–30°N displayed more temporally heterogeneous responses. The nonlocal effects north of 30°N were dominated by cooling, with the strongest cooling (≥2 K) between March and June in the 50°N–60°N zone. Beyond 60°N, moderate warming was detected from November to January.

There were notable differences in the magnitude and seasonality of nonlocal effects across methods. For instance, the Land-only Subgrid produced slightly stronger low-latitude warming than the Coupled Subgrid (Figures 5b and 5c). The Checkerboard and Window Regression produced weak, spatially mixed warming signals in the tropics (Figures 5d and 5g). The IBPM, in contrast, detected sporadic warming in the Northern Hemisphere during winter months (Figure 5f). By comparison, the Spectral Separation revealed a persistent and significant cooling signal in the Southern Hemisphere.

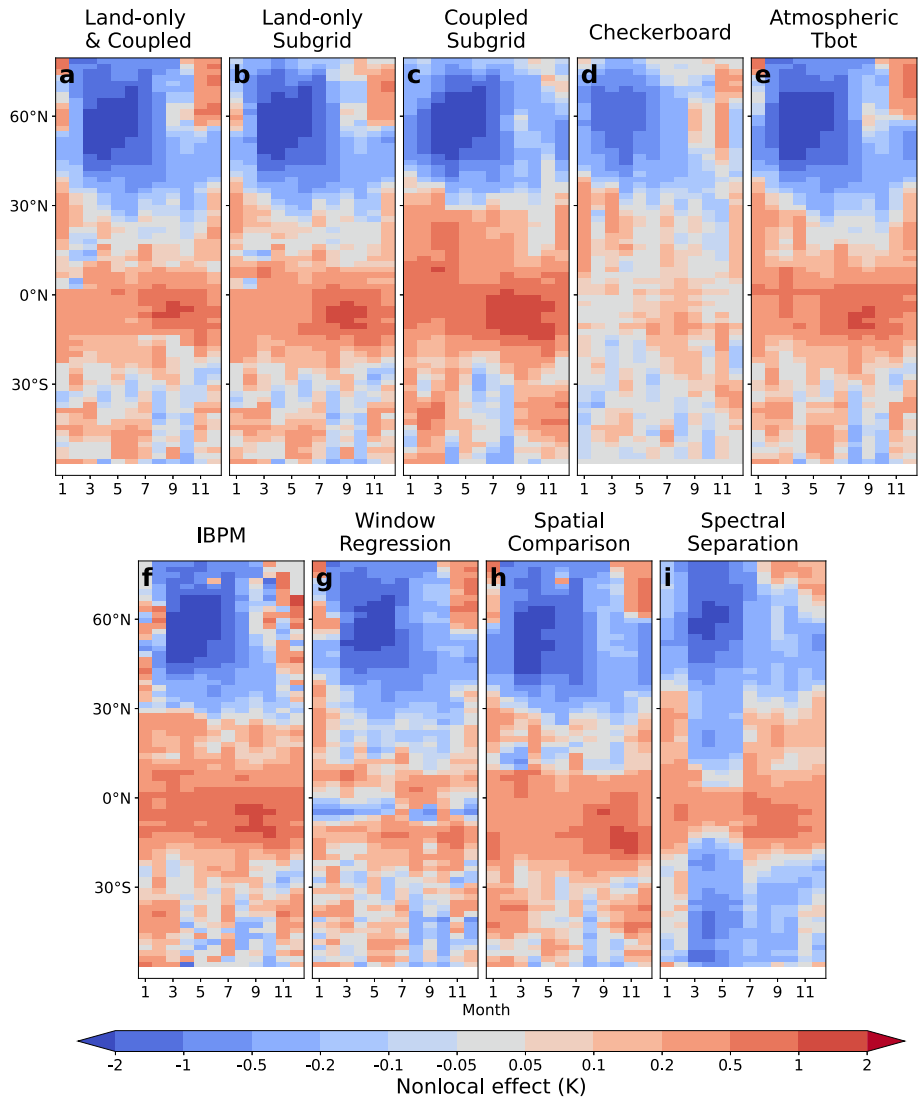


**Figure 5.** Seasonal and latitudinal variations of nonlocal effects from methods (a–i).

### 3.3. Inter-Method Consistency in the Local and Nonlocal Effects

We quantified the sign agreement of the separated local and nonlocal effects across the methods described above. Local effects exhibited complete sign agreement (9/9) in 34.9% of the global LCC grids (Figure 6a). In comparison, nonlocal effects reached complete agreement in 46.2% of global land grids (Figure 6b). Zonally, both local and nonlocal effects showed a sign agreement greater than 7/9 across most latitude bands (Figure 6c). Specifically, the warming-dominated tropical regions and the cooling-dominated northern high latitudes displayed higher agreement. In contrast, mid-latitude regions in the Northern Hemisphere showed lower agreement due to variations in the transition latitudes that separate warming and cooling. In the mid-latitudes of the Southern Hemisphere, the reduced consistency likely resulted from a limited sample size.

We also evaluated the consistency of local and nonlocal effects in spatial patterns and magnitude among methods using the symmetric index of agreement ($\lambda$; higher values are better) (Figure S5 in Supporting Information S1). Results indicated a generally robust consistency across all methods, but noticeable differences between specific methods (Table S2 in Supporting Information S1). For local effects, inter-method λ values ranged from 0.39 to 0.98. The IBPM showed the lowest consistency (mean $\lambda = 0.53$), whereas the Land-only and Coupled exhibited relatively higher consistency (mean $\lambda = 0.77$). For nonlocal effects, λ ranged from 0.53 to 0.98. The Atmospheric

10.1029/2025EF007704

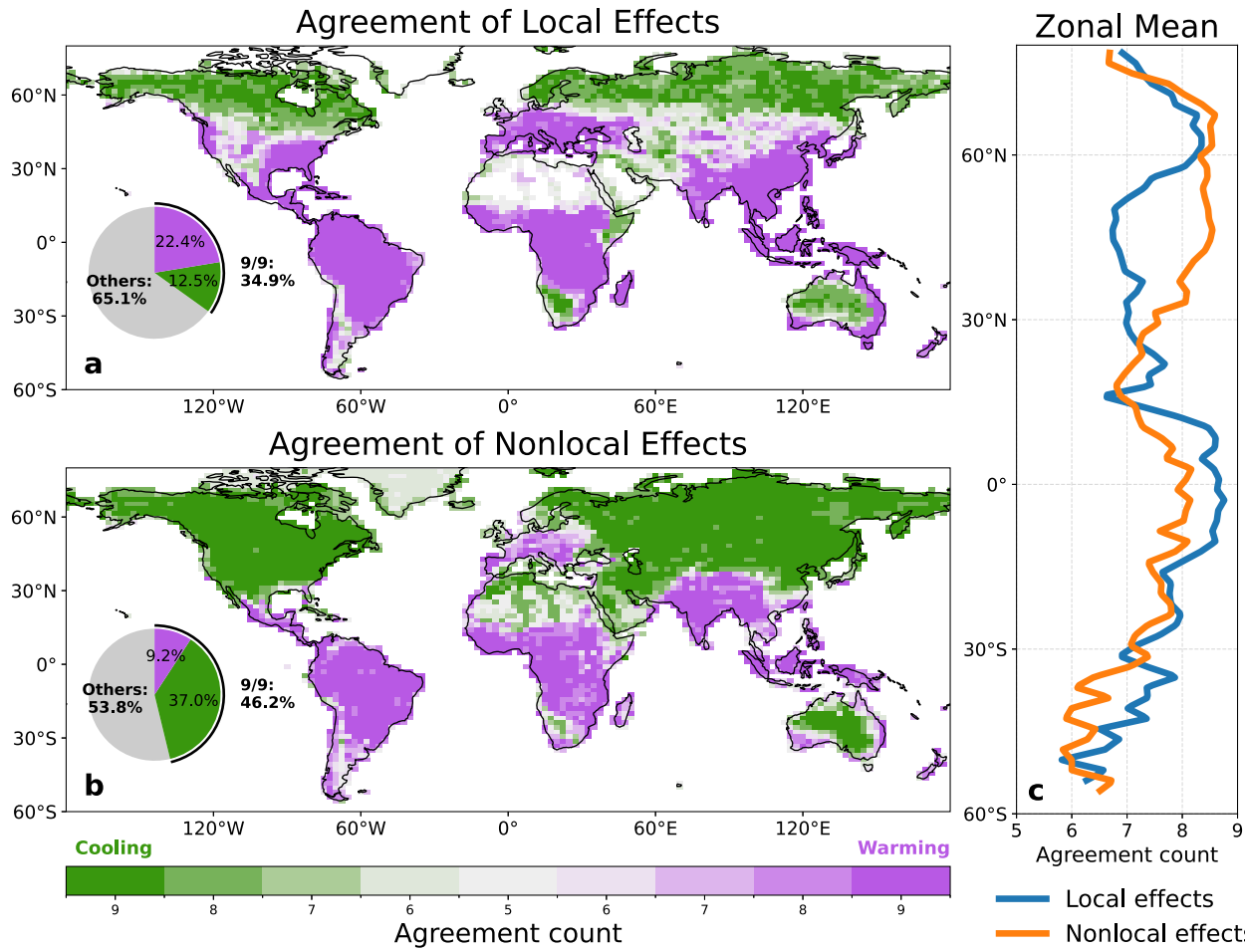


**Figure 6.** Sign agreement between different methods for local (a) and nonlocal effects (b) and their latitudinal variations (c). The sign agreement is expressed as the count of signs that agree with the majority sign across all methods. The inset pie charts illustrate the proportions of grid points that show complete agreement (9 out of 9) for warming and cooling, respectively.

Tbot yielded relatively high consistency (mean $\lambda = 0.84$), likely because its directly estimated nonlocal effects are more stable. In contrast, interpolation biases in the Checkerboard method resulted in the lowest mean λ (0.62).

## 4. Discussion

### 4.1. The Intercomparison and Recommendation of Different Methods

All separation methods we considered are applicable for quantifying local and nonlocal effects, with broad consensus, and each has its own methodological assumptions and data requirements. Based on intercomparison results, we discuss each method's capacity, strengths, and limitations, and offer practical guidance for users to choose appropriate methods based on specific research objectives and data availability, as summarized in Table 3.

Traditional sensitivity experiments that rely on different land-cover scenarios capture only the total effects of LCC. However, the local and nonlocal effects can be isolated from additional simulations (a total of four experiments in our case), which has a computational cost.

For models that support subgrid outputs for different land cover or PFT types, one can directly extract local effects from PFT differences using a single land-only experiment (Equation 1) based on the space-for-time analogy. With a coupled LCC experiment, nonlocal effects can be quantified by climate differences of the same PFT relative to the CTL experiment (Equation 2). However, the selection of the reference experiment (CTL or DEF) by which PFT differences are extracted as local effects may influence the results, because of the differences in background climate between the CTL and DEF experiments (X. Liu et al., 2023). The subtle differences between the isolated

Earth's Future

10.1029/2025EF007704

**Table 3**
*Summary of Strengths and Limitations of Each Method for Quantifying Local and Nonlocal Effects of Land Cover Changes*

| Methods | Description | Advantages | Disadvantages |
|---|---|---|---|
| (1) Land-only and Coupled | – Sensitivity experiments of different land cover change scenarios<br>– Local and nonlocal effects separated from the total effects via land-only and coupled simulations | – Applicable to all climate models | – Require four dedicated designed experiments<br>– Relatively high computational cost |
| (2) Subgrid | – Subgrid PFTs within a model grid share the same atmospheric forcing and their differences reflect the local effects (land-only or coupled)<br>– Differences of the same PFT between scenarios reflect the nonlocal effects (coupled) | – Analogous to space-for-time method with good comparability<br>– Most consistent with definitions of local and nonlocal effects<br>– Applicable to other subgrid land variables<br>– Require fewer experiments | – Only for models with proper representation of subgrid processes and outputs |
| (3) Checkerboard | – Climate model simulations under "Checkerboard" land cover change scenarios<br>– Local and nonlocal effects obtained by spatial interpolation | – Applicable to different land and atmospheric variables without variable-specific physical assumptions | – Requires customized checkerboard experiments<br>– Checkerboard design and layout affect results<br>– Nonlocal effects are sensitive to spatial extent of LCC<br>– Potential interpolation artifacts |
| (4) Atmospheric Tbot | – Using bottom atmospheric air temperature changes as nonlocal effects, assuming similar responses to surface temperature<br>– Local effects obtained as residue of nonlocal effects from total effects | – Easily applicable to all climate models | – Strong assumptions<br>– Applicability requires further validation |
| (5) IBPM | – Analytical solution to approximate the local effects of land cover change by biophysical changes, which is derived from energy balance equations assuming no atmospheric feedback<br>– Nonlocal effects obtained as the residual of local effects from total effects | – A post-processing technique applicable to climate model output and empirical data<br>– Enable decomposing local effects to contributions of different biophysical factors | – Omitting higher-order terms results in outliers and errors<br>– Estimation of biophysical factors contains large uncertainty (e.g., aerodynamic resistance in high latitudes)<br>– Only applicable to LST |
| (6) Window Regression | – Constructs a multiple linear regression model using samples within a moving window<br>– Separate the LCC-induced local effects via the regression coefficient and attribute the remaining signal to nonlocal effects. | – A post-processing technique applicable to climate model output and empirical data | – Results sensitive to samples within the regression window<br>– Linear models are limited in capturing nonlinear and interactive effects among variables |
| (7) Spatial Comparison | – Compare high- and low-LCC grids, or LCC and non-LCC grids using an adaptive moving window, and attribute their differences as local effects<br>– Nonlocal effects derived as the residual from the total effects. | – A post-processing technique applicable to climate model output and empirical data | – Subjective criterion for selecting LCC and non-LCC grids<br>– Results sensitive to the choice of parameters (distance, threshold, window size) |
| (8) Spectral Separation | – Harmonic–based spectral signal separation<br>– Local and nonlocal effects derived from small- and large- scale spectral components using modulation | – A post-processing technique applicable to climate model output with less spatial assumptions<br>– Scale-aware and additive separation | – Spurious local effect signals in non-LCC regions due to spectral spreading<br>– Sensitive to modulation rule and spectral parameters<br>– Difficult to interpret |

nonlocal effects from land-only and coupled sensitivity experiments (Figures S2a and S2b in Supporting Information S1) likely result from the distinct atmospheric background conditions, as the latter includes feedback. Moreover, some model-related technical issues, for example, the shared soil column in CLM (Meier et al., 2018; Schultz et al., 2016), may affect the validity of the assumption that subgrid PFTs are independent and differ only in biophysical properties.

The nonlocal and total effects in the Checkerboard method were significantly weaker than those of other methods, while the local effects remained comparable. This is because the imposed partial deforestation in the checkerboard scenario was only half that of the complete global deforestation in other methods. Since nonlocal effects are more sensitive to the spatial extent of land cover changes than local effects, the sparse and extensive LCC and their grid size influence the strength of nonlocal effects due to the scale-dependency (Winckler et al., 2017a). The reconstruction of local and nonlocal effects could yield a stronger local and total signal due to interpolation artifacts (De Hertog et al., 2023; Jäger et al., 2025). Therefore, the interpretation of the relative strength of local and nonlocal effects should account for these issues. Moreover, the interpolated local and nonlocal effects are influenced by different checkerboard layouts and subject to high uncertainty near the edges of LCC due to a lack of reference grids (e.g., the Sahara in our case). This means that the spatial distribution of land cover in the real world, especially when it is scattered and unevenly distributed, may affect the effectiveness of this method. It is crucial to create a proper checkerboard design that balances the intended LCC pattern while maintaining sufficient and representative samples to ensure the accuracy of spatial interpolation. An advantage of the Checkerboard method is that it does not rely on variable-specific physical assumptions, making it extendable to other climate variables (such as precipitation (Winckler et al., 2017a), cloud cover (Hua et al., 2023)). Similar extensions are also possible for other methods, like the Window Regression, Spatial Comparison, and Spectral Separation. Even without a dedicated checkerboard LCC design, there have been attempts to directly apply the spatial interpolation strategy, the essence of the Checkerboard method, to historical LCC experiments (Hua et al., 2023). However, the accuracy of this interpolation approach is compromised by the spatial sampling and representativeness of the historical LCC pattern, and careful selection of these regions is required in practical applications.

The Atmospheric Tbot method utilizes the bottom-level atmospheric temperature changes as nonlocal effects, which closely aligns with the definition of nonlocal effects. It assumes that the changes in bottom atmospheric air temperature, near-surface air temperature, and land surface temperature in response to LCC are similar, ignoring potential changes in the vertical profile and physical differences among these temperature metrics. Our analyses support the broad validity of this assumption (Figure S2a in Supporting Information S1), and the results demonstrated stable performance in separating local and nonlocal effects. Since local effects in this method are obtained as the residual of the total effects, the relative magnitudes of local and nonlocal effects may affect its performance. The strength of this method lies in its simplicity; however, it cannot explain the physical mechanisms underlying those effects. Moreover, the applicability of this method for different land cover change scenarios and models needs further verification.

The IBPM method is a mathematical derivation of energy balance equations. It quantifies the local LST changes by LCC by summing contributions of different biophysical factors (albedo, Bowen ratio, and aerodynamic resistance), assuming an atmospheric state unaffected by LCC. However, the land cover changes in our experiments are large enough to substantially alter atmospheric conditions, which in turn may affect the estimation of several contribution terms (e.g., Bowen ratio and aerodynamic resistance) (Bright et al., 2017; Ge et al., 2019). Mathematically, the IBPM derivation is an approximate solution that neglects higher-order and interaction terms. These omissions can give rise to outliers under certain conditions (Chen et al., 2022; Liao et al., 2018), which affect the accuracy of IBPM in reproducing local effects, particularly in high-latitude regions. Other variants of IBPM with different derivations have been proposed, such as the Two-Resistance Mechanism, which considers higher-order terms (Rigden & Li, 2017) and that incorporates additional climate variables and explicitly considers the 2-m air temperature (Zeng et al., 2017).

The Window Regression method estimates local effects by using the regression slope of temperature changes on the LCC fraction, controlling for geographical factors. Such estimation is influenced by the size of the moving window, the sampling number and density, as well as spatial variations in background climatic and geographical conditions. More advanced regression treatments, such as singular value decomposition (Duveiller et al., 2018a) and ridge regression (Huang et al., 2020), have been introduced to enhance robustness. Among these factors, the

choice of window is key to ensuring the representativeness of the target grid cells within it. An overly large window may smooth out local signals and hinder their identification, whereas a too small window may lead to unstable estimates due to insufficient samples (Duveiller et al., 2021). Moreover, since the regression slope represents the potential effect under a 100% LCC, the actual local effects at each grid cell must be multiplied by its land cover change fraction. The data-driven method enables estimating climate responses across varying levels of LCC without requiring additional scenario-based simulations.

The Spatial Comparison method extracts the local effects of LCCs by comparing LCC-affected grids with nearby undisturbed grids, assuming a similar background climate within the search window. As with the Window Regression method, a key aspect is defining the search window for comparison. Compared to fixed-size windows, dynamically adjusting windows expand their size to include more samples, thereby improving spatial coverage and the effectiveness of comparisons in regions with spatially inhomogeneous patterns of LCC. Moreover, the method's success depends strongly on how effectively it suppresses confounding non-LCC factors (such as climatic noise and topographic effects) while simultaneously highlighting the LCC signal. In practical applications, it is essential to design adaptive spatial searching and robust control strategies to enhance the generalizability and accuracy of the approach for a specific study context (Chen et al., 2024; Li et al., 2015).

The Spectral Separation method separates local and nonlocal effects based on their characteristic spatial scales in the decomposed spectral domain. As a post-processing approach, it does not require specially designed experiments or spatial assumptions like other methods. Nevertheless, it is constrained by inherent limitations of spectral methods (Jäger et al., 2025). The lack of explicit spatial constraints may introduce spurious local effects in non-LCC regions. The accuracy of signal separation is sensitive to grid-scale forcing patterns and the choice of modulation rule and parameters. Also, interpreting the spectral decomposition results is not straightforward for users unfamiliar with spherical harmonics.

### 4.2. Shared Methodological Challenges in the Separation of Local and Nonlocal Effects

In addition to method-specific discussion, several shared conceptual challenges in separately quantifying the local and nonlocal effects warrant further discussion.

*Model simulation and observation differences*. While there are broadly consistent global patterns, the local effects in the climate model also show regional differences compared to the observational benchmark. These differences arise from multiple sources. On the simulation side, these include biases and uncertainties in the model's representation of biophysical processes (Danabasoglu et al., 2020; Lian et al., 2018), the emissivity used to back-calculate modeled LST (Jin & Liang, 2006), and time-resolution dependent conversion of emitted longwave radiation to LST due to their non-linear relationship. More importantly, the structural model uncertainty and internal variability (Boysen et al., 2020; Jäger et al., 2026; Pitman et al., 2009) are particularly relevant for the interpretation of nonlocal signals given the limited ensemble size, because they may cause the large inter-model spread of the simulated nonlocal effects (S. Liu et al., 2023; Luo et al., 2024; Winckler, Reick, et al., 2019). On the observation side, benchmark data are restricted to Earth's current land cover distribution, thereby limiting their spatial coverage. Further, observations can be subject to temporal gaps. For example, satellite LST can be retrieved only under clear-sky conditions. Evaluating local effects against observations should account for the observational data sets' uncertainties and methodological differences. Sensor and algorithm errors in observations also matter. Data from model simulations can be post-processed better to match the availability or constraints of observational data. For example, model data can be masked for clear-sky conditions when comparing to satellite LST data (Meier et al., 2022).

*Influence of background climate conditions*. Background climate conditions (e.g., temperature, precipitation, and snow cover) regulate biophysical factors that affect the radiative and non-radiative processes of land cover change (Pitman et al., 2011; Verbiest et al., 2023; Winckler et al., 2017b). In our study, the distinct climate differences between the land-only and coupled experiments (GSWP forcing vs. simulated atmosphere) reflect the LCC-triggered atmospheric feedback, which, in turn, affects the local effects by altered biophysical factors. For example, the selection of reference experiments (CTL or DEF) used by the Subgrid and IBPM methods influences the estimated local effects because snow cover, albedo, and other factors differ between experiments. Our sensitivity experiments employed cycling forcing around year 2000 to stabilize the background climate condition. Background climate conditions in transient climate simulations, which often involve changing various internal and external forcings (Jäger et al., 2026), show long-term changes (e.g., LUMIP). Elucidating how local effects

vary under background climate changes induced by LCC or greenhouse gas forcing could improve method comparability and inform the likely changes in biophysical effects under future climate (Li, Ge, et al., 2025; Pitman et al., 2011).

*The interdependence of local and nonlocal effects*. In our study, many separation methods estimate local or nonlocal effects as the residual of the nonlocal/local component from the total effects. This treatment implicitly assumes that the local and nonlocal effects are independent, with no interaction between them. However, the independent assumption may not be strictly valid. This could be one of the reasons why the reconstructed total effects (the sum of the separated local and nonlocal effects) differed from the original total effects (Figures S3 and S4 in Supporting Information S1). Some interactions may occur between local and nonlocal effects due to their reciprocal interaction between land and atmosphere. However, the degree of their interdependence remains insufficiently studied.

*Application to other climate variables*. Local and nonlocal effects of LCC are not only present in temperature changes but also in other climate variables (precipitation, clouds, etc.). This study focuses on the LST variable for method comparison purposes. Other temperature variables (e.g., 2-m air temperature) also respond to LCC, and their responses may differ from that of LST (Li, Li, et al., 2025; Novick & Katul, 2020; Winckler, Reick, et al., 2019) (Figure S2b in Supporting Information S1). The near-surface temperature, particularly the 2m air temperature ($T_{2m}$), is a key indicator of climate change and of climate mitigation targets. Expanding the separation methods to work for more climate variables (some methods in our study are applicable to $T_{2m}$ and others; see Table 3) beyond temperature would be an important next step and would help diagnose uncertainty sources in the climate response to land cover change across different models, such as LUMIP (S. Liu et al., 2023; Luo et al., 2024).

## 5. Conclusions

This study quantifies the biophysical impacts of LCC through global deforestation experiments and evaluates multiple methods for separating the simulated land surface temperature changes into local and nonlocal components. Our intercomparison analyses reveal that the local and nonlocal effects separated by different methods are broadly consistent in magnitude and spatial pattern. However, regional differences arise from each method's methodological assumptions. By identifying the applicability and limitations of each method, we provide guidance on effectively disentangling local and nonlocal effects in practical contexts. Further research could focus on extending the applications of separation methods to additional climate variables and other climate models and experiments. Moreover, examining the interactions between local and nonlocal effects, accounting for the modulation of background climate conditions on local effects, and developing more accurate separation methodologies would deepen our understanding of these multiscale climatic impacts of LCC. These efforts would also help improve the representation of biophysical processes and land–atmosphere feedbacks in developing Earth system models.

## Conflict of Interest

The authors declare no conflicts of interest relevant to this study.

## Availability Statement

All code and model output data necessary for reproducing the results of this study are available on Figshare (Zhao & Li, 2026). ETOPO1 global relief data were obtained from NOAA National Geophysical Data Center (2009). The Li2015 data set is available from Li (2021), and the Duveiller2018 data set is available from Duveiller et al. (2018b).

**Acknowledgments**
This study is supported by the National Natural Science Foundation of China (Grant 42371102) and the 111 Project of China (Grant B23027). We thank the technical support of the National Large Scientific and Technological Infrastructure "Earth System Numerical Simulation Facility" (https://cstr.cn/31134.02.EL) for this work.

## References

Alkama, R., & Cescatti, A. (2016). Biophysical climate impacts of recent changes in global forest cover. *Science*, *351*(6273), 600–604. https://doi.org/10.1126/science.aac8083

Amali, A. A., Schwingshackl, C., Ito, A., Barbu, A., Delire, C., Peano, D., et al. (2025). Biogeochemical versus biogeophysical temperature effects of historical land-use change in CMIP6. *Earth System Dynamics*, *16*(3), 803–840. https://doi.org/10.5194/esd-16-803-2025

Bathiany, S., Claussen, M., Brovkin, V., Raddatz, T., & Gayler, V. (2010). Combined biogeophysical and biogeochemical effects of large-scale forest cover changes in the MPI Earth system model. *Biogeosciences*, *7*(5), 1383–1399. https://doi.org/10.5194/bg-7-1383-2010

Boisier, J. P., De Noblet-Ducoudré, N., Pitman, A. J., Cruz, F. T., Delire, C., Van Den Hurk, B. J. J. M., et al. (2012). Attributing the impacts of land-cover changes in temperate regions on surface temperature and heat fluxes to specific causes: Results from the first LUCID set of simulations. *Journal of Geophysical Research*, *117*, 2011JD017106. https://doi.org/10.1029/2011JD017106

Boysen, L. R., Brovkin, V., Arora, V. K., Cadule, P., de Noblet-Ducoudré, N., Kato, E., et al. (2014). Global and regional effects of land-use change on climate in 21st century simulations with interactive carbon cycle. *Earth System Dynamics*, *5*(2), 309–319. https://doi.org/10.5194/esd-5-309-2014

Boysen, L. R., Brovkin, V., Pongratz, J., Lawrence, D. M., Lawrence, P., Vuichard, N., et al. (2020). Global climate response to idealized deforestation in CMIP6 models. *Biogeosciences*, *17*(22), 5615–5638. https://doi.org/10.5194/bg-17-5615-2020

Bright, R. M., Davin, E., O'Halloran, T., Pongratz, J., Zhao, K., & Cescatti, A. (2017). Local temperature response to land cover and management change driven by non-radiative processes. *Nature Climate Change*, *7*(4), 296–302. https://doi.org/10.1038/nclimate3250

Chalita, S., & Le Treut, H. (1994). The albedo of temperate and boreal forest and the northern hemisphere climate: A sensitivity experiment using the LMD GCM. *Climate Dynamics*, *10*(4–5), 231–240. https://doi.org/10.1007/BF00208990

Chen, C., Ge, J., Guo, W., Cao, Y., Liu, Y., Luo, X., & Yang, L. (2022). The biophysical impacts of idealized afforestation on surface temperature in China: Local and nonlocal effects. *Journal of Climate*, *35*(23), 7833–7852. https://doi.org/10.1175/jcli-d-22-0144.1

Chen, C., Li, Y., Wang, X., Luo, X., Li, Y., Cheng, Y., & Zhu, Z. (2024). Biophysical effects of croplands on land surface temperature. *Nature Communications*, *15*(1), 10901. https://doi.org/10.1038/s41467-024-55319-2

Chen, H., Hua, W., Zhu, S., Liu, S., & Chen, H. (2026). Contrasting responses of near-surface air temperature to historical land cover change in CESM. *Advances in Atmospheric Sciences*, *43*(4), 827–844. https://doi.org/10.1007/s00376-025-5058-5

Chen, L., & Dirmeyer, P. A. (2016). Adapting observationally based metrics of biogeophysical feedbacks from land cover/land use change to climate modeling. *Environmental Research Letters*, *11*(3), 034002. https://doi.org/10.1088/1748-9326/11/3/034002

Chen, L., & Dirmeyer, P. A. (2020). Reconciling the disagreement between observed and simulated temperature responses to deforestation. *Nature Communications*, *11*(1), 202. https://doi.org/10.1038/s41467-019-14017-0

Claussen, M., Brovkin, V., & Ganopolski, A. (2001). Biogeophysical versus biogeochemical feedbacks of large-scale land cover change. *Geophysical Research Letters*, *28*(6), 1011–1014. https://doi.org/10.1029/2000GL012471

Cui, X., & Graf, H.-F. (2009). Recent land cover changes on the Tibetan Plateau: A review. *Climate Change*, *94*(1–2), 47–61. https://doi.org/10.1007/s10584-009-9556-8

Danabasoglu, G., Lamarque, J.-F., Bacmeister, J., Bailey, D. A., DuVivier, A. K., Edwards, J., et al. (2020). The community Earth system model version 2 (CESM2). *Journal of Advances in Modeling Earth Systems*, *12*, e2019MS001916. https://doi.org/10.1029/2019MS001916

De Hertog, S. J., Havermann, F., Vanderkelen, I., Guo, S., Luo, F., Manola, I., et al. (2023). The biogeophysical effects of idealized land cover and land management changes in Earth system models. *Earth System Dynamics*, *14*(3), 629–667. https://doi.org/10.5194/esd-14-629-2023

Devaraju, N., Bala, G., & Modak, A. (2015). Effects of large-scale deforestation on precipitation in the monsoon regions: Remote versus local effects. *Proceedings of the National Academy of Sciences*, *112*(11), 3257–3262. https://doi.org/10.1073/pnas.1423439112

Devaraju, N., De Noblet-Ducoudré, N., Quesada, B., & Bala, G. (2018). Quantifying the relative importance of direct and indirect biophysical effects of deforestation on surface temperature and teleconnections. *Journal of Climate*, *31*, 3811–3829. https://doi.org/10.1175/jcli-d-17-0563.1

Di Vittorio, A. V., Mao, J., Shi, X., Chini, L., Hurtt, G., & Collins, W. D. (2018). Quantifying the effects of historical land cover conversion uncertainty on global carbon and climate estimates. *Geophysical Research Letters*, *45*(2), 974–982. https://doi.org/10.1002/2017GL075124

Duveiller, G., Fasbender, D., & Meroni, M. (2016). Revisiting the concept of a symmetric index of agreement for continuous datasets. *Scientific Reports*, *6*(1), 19401. https://doi.org/10.1038/srep19401

Duveiller, G., Filipponi, F., Ceglar, A., Bojanowski, J., Alkama, R., & Cescatti, A. (2021). Revealing the widespread potential of forests to increase low level cloud cover. *Nature Communications*, *12*(1), 4337. https://doi.org/10.1038/s41467-021-24551-5

Duveiller, G., Hooker, J., & Cescatti, A. (2018a). A dataset mapping the potential biophysical effects of vegetation cover change. *Scientific Data*, *5*(1), 180014. https://doi.org/10.1038/sdata.2018.14

Duveiller, G., Hooker, J., & Cescatti, A. (2018b). A dataset mapping the potential biophysical effects of vegetation cover change. *Figshare*. [Dataset]. https://doi.org/10.6084/m9.figshare.c.3829333

Ge, J., Guo, W., Pitman, A. J., Kauwe, M. G. D., Chen, X., & Fu, C. (2019). The nonradiative effect dominates local surface temperature change caused by afforestation in China. https://doi.org/10.1175/JCLI-D-18-0772.1

Gibbard, S., Caldeira, K., Bala, G., Phillips, T. J., & Wickett, M. (2005). Climate effects of global land cover change. *Geophysical Research Letters*, *32*(23). https://doi.org/10.1029/2005GL024550

Hansen, M. C., Stehman, S. V., & Potapov, P. V. (2010). Quantification of global gross forest cover loss. *Proceedings of the National Academy of Sciences*, *107*(19), 8650–8655. https://doi.org/10.1073/pnas.0912668107

Hua, W., Zhou, L., Dai, A., Chen, H., & Liu, Y. (2023). Important non-local effects of deforestation on cloud cover changes in CMIP6 models. *Environmental Research Letters*, *18*(9), 094047. https://doi.org/10.1088/1748-9326/acf232

Huang, B., Hu, X., Fuglstad, G.-A., Zhou, X., Zhao, W., & Cherubini, F. (2020). Predominant regional biophysical cooling from recent land cover changes in Europe. *Nature Communications*, *11*(1), 1066. https://doi.org/10.1038/s41467-020-14890-0

Intergovernmental Panel On Climate Change. (2022). Climate change and land: IPCC special report on climate change, desertification, land degradation. In *Sustainable land management, food security, and greenhouse gas fluxes in terrestrial ecosystems* (1st ed.). Cambridge University Press. https://doi.org/10.1017/9781009157988

Jäger, F., Schwaab, J., Bukenberger, M., De Hertog, S. J., & Seneviratne, S. I. (2025). Spectral decomposition and signal separation of climate responses to land cover changes. *Journal of Geophysical Research: Atmospheres*, *130*(5), e2024JD042698. https://doi.org/10.1029/2024JD042698

Jäger, F., Sieber, P., Simpson, I. R., Lawrence, P., Lawrence, D., & Seneviratne, S. I. (2026). On the robustness of modeled non-local temperature effects of historical land use changes. *Journal of Advances in Modeling Earth Systems*, *18*(2), e2025MS005227. https://doi.org/10.1029/2025MS005227

Jin, M., & Liang, S. (2006). An improved land surface emissivity parameter for land surface models using global remote sensing observations. *Journal of Climate*, *19*(1), 2867–2881. https://doi.org/10.1175/jcli3720.1

Kan, F., Xu, H., Tang, S., Peñuelas, J., Lian, X., Roebroek, C. T. J., et al. (2025). Diminished biophysical cooling benefits of global forestation under rising atmospheric CO2. *Nature Communications*, *16*(1), 4410. https://doi.org/10.1038/s41467-025-59547-y

Kumar, S., Dirmeyer, P. A., Merwade, V., DelSole, T., Adams, J. M., & Niyogi, D. (2013). Land use/cover change impacts in CMIP5 climate simulations: A new methodology and 21st century challenges. *Journal of Geophysical Research: Atmospheres*, *118*(12), 6337–6353. https://doi.org/10.1002/jgrd.50463

Lawrence, D., Coe, M., Walker, W., Verchot, L., & Vandecar, K. (2022). The unseen effects of deforestation: Biophysical effects on climate. *Frontiers in Forests and Global Change*, *5*, 756115. https://doi.org/10.3389/ffgc.2022.756115

Lawrence, D. M., Fisher, R. A., Koven, C. D., Oleson, K. W., Swenson, S. C., Bonan, G., et al. (2019). The community land model version 5: Description of new features, benchmarking, and impact of forcing uncertainty. *Journal of Advances in Modeling Earth Systems*, *11*(12), 4245–4287. https://doi.org/10.1029/2018MS001583

Lawrence, D. M., Hurtt, G. C., Arneth, A., Brovkin, V., Calvin, K. V., Jones, A. D., et al. (2016). The land use model intercomparison project (LUMIP) contribution to CMIP6:rationale and experimental design. *Geoscientific Model Development*, *9*, 2973–2998. https://doi.org/10.5194/gmd-9-2973-2016

Lee, X., Goulden, M. L., Hollinger, D. Y., Barr, A., Black, T. A., Bohrer, G., et al. (2011). Observed increase in local cooling effect of deforestation at higher latitudes. *Nature*, *479*(7373), 384–387. https://doi.org/10.1038/nature10588

Lejeune, Q., Davin, E. L., Gudmundsson, L., Winckler, J., & Seneviratne, S. I. (2018). Historical deforestation locally increased the intensity of hot days in northern mid-latitudes. *Nature Climate Change*, *8*(5), 386–390. https://doi.org/10.1038/s41558-018-0131-z

Lejeune, Q., Seneviratne, S. I., & Davin, E. L. (2017). Historical land-cover change impacts on climate: Comparative assessment of LUCID and CMIP5 multimodel experiments. *Journal of Climate*, *30*(4), 1439–1459. https://doi.org/10.1175/jcli-d-16-0213.1

Li, Y. (2021). Dataset for paper "Local cooling and warming effects of forest based on satellite data.". *Figshare*. [Dataset]. https://doi.org/10.6084/m9.figshare.2445310.v4

Li, Y., Ge, J., Wu, H., Tang, R., Cheng, Y., Liu, X., et al. (2025). Amplified local cooling effect of forestation in warming Europe. *Nature Communications*, *16*(1), 8412. https://doi.org/10.1038/s41467-025-63556-2

Li, Y., Li, Z.-L., Wu, H., Liu, X., Lian, X., Si, M., et al. (2025). Observed different impacts of potential tree restoration on local surface and air temperature. *Nature Communications*, *16*(1), 2335. https://doi.org/10.1038/s41467-025-57606-y

Li, Y., Xu, R., Yang, K., Liu, Y., Wang, S., Zhou, S., et al. (2023). Contribution of Tibetan Plateau ecosystems to local and remote precipitation through moisture recycling. *Global Change Biology*, *29*(3), 702–718. https://doi.org/10.1111/gcb.16495

Li, Y., Xu, R., Yang, Z., Zhou, S., Lu, M., Lin, H., et al. (2024). Upwind moisture controls on interannual variations of precipitation and vegetation in China's drylands. *Geophysical Research Letters*, *51*(18), e2024GL110997. https://doi.org/10.1029/2024gl110997

Li, Y., Zhao, M., Motesharrei, S., Mu, Q., Kalnay, E., & Li, S. (2015). Local cooling and warming effects of forests based on satellite observations. *Nature Communications*, *6*(1), 6603. https://doi.org/10.1038/ncomms7603

Lian, X., Piao, S., Huntingford, C., Li, Y., Zeng, Z., Wang, X., et al. (2018). Partitioning global land evapotranspiration using CMIP5 models constrained by observations. *Nature Climate Change*, *8*(7), 640–646. https://doi.org/10.1038/s41558-018-0207-9

Liao, W., Rigden, A. J., & Li, D. (2018). Attribution of local temperature response to deforestation. *Journal of Geophysical Research: Biogeosciences*, *123*(5), 1572–1587. https://doi.org/10.1029/2018jg004401

Liu, S., Hua, W., Zhou, L., Chen, H., Yu, M., Li, X., & Cui, Y. (2023). Local and non-local biophysical impacts of deforestation on global temperature during boreal summer: CMIP6-LUMIP multimodel analysis. *Journal of Geophysical Research: Atmospheres*, *128*(11), e2022JD038229. https://doi.org/10.1029/2022jd038229

Liu, X., Li, Z.-L., Li, Y., Wu, H., Zhou, C., Si, M., et al. (2023). Local temperature responses to actual land cover changes present significant latitudinal variability and asymmetry. *Scientific Bulletin*, *68*(22), 2849–2861. https://doi.org/10.1016/j.scib.2023.09.046

Luo, X., Ge, J., Cao, Y., Liu, Y., Yang, L., Wang, S., & Guo, W. (2024). Local and nonlocal biophysical effects of historical land use and land cover changes in CMIP6 models and the intermodel uncertainty. *Earth's Future*, *12*(6), e2023EF004220. https://doi.org/10.1029/2023EF004220

Luyssaert, S., Jammet, M., Stoy, P. C., Estel, S., Pongratz, J., Ceschia, E., et al. (2014). Land management and land-cover change have impacts of similar magnitude on surface temperature. *Nature Climate Change*, *4*(5), 389–393. https://doi.org/10.1038/nclimate2196

Malyshev, S., Shevliakova, E., Stouffer, R. J., & Pacala, S. W. (2015). Contrasting local versus regional effects of land-use-change-induced heterogeneity on historical climate: Analysis with the GFDL Earth system model. *Journal of Climate*, *28*(13), 5448–5469. https://doi.org/10.1175/JCLI-D-14-00586.1

Meier, R., Davin, E. L., Bonan, G. B., Lawrence, D. M., Hu, X., Duveiller, G., et al. (2022). Impacts of a revised surface roughness parameterization in the community land model 5.1. *Geoscientific Model Development*, *15*(6), 2365–2393. https://doi.org/10.5194/gmd-15-2365-2022

Meier, R., Davin, E. L., Lejeune, Q., Hauser, M., Li, Y., Martens, B., et al. (2018). Evaluating and improving the community land Model's sensitivity to land cover. *Biogeosciences*, *15*, 4731–4757. https://doi.org/10.5194/bg-15-4731-2018

NOAA National Geophysical Data Center. (2009). ETOPO1 1 arc-minute global relief model. *NOAA National Centers for Environmental Information*. [Dataset]. https://doi.org/10.7289/v5c8276m

Novick, K. A., & Katul, G. G. (2020). The duality of reforestation impacts on surface and air temperature. *Journal of Geophysical Research: Biogeosciences*, *125*(4), e2019JG005543. https://doi.org/10.1029/2019jg005543

Pitman, A. J., Avila, F. B., Abramowitz, G., Wang, Y. P., Phipps, S. J., & de Noblet-Ducoudré, N. (2011). Importance of background climate in determining impact of land-cover change on regional climate. *Nature Climate Change*, *1*(9), 472–475. https://doi.org/10.1038/nclimate1294

Pitman, A. J., De Noblet-Ducoudré, N., Cruz, F. T., Davin, E. L., Bonan, G. B., Brovkin, V., et al. (2009). Uncertainties in climate responses to past land cover change: First results from the LUCID intercomparison study. *Geophysical Research Letters*, *36*, 2009GL039076. https://doi.org/10.1029/2009GL039076

Pongratz, J., Schwingshackl, C., Bultan, S., Obermeier, W., Havermann, F., & Guo, S. (2021). Land use effects on climate: Current state, recent progress, and emerging topics. *Current Climate Change Reports*, *7*(4), 99–120. https://doi.org/10.1007/s40641-021-00178-y

Portmann, R., Beyerle, U., Davin, E., Fischer, E. M., De Hertog, S., & Schemm, S. (2022). Global forestation and deforestation affect remote climate via adjusted atmosphere and ocean circulation. *Nature Communications*, *13*(1), 5569. https://doi.org/10.1038/s41467-022-33279-9

Prevedello, J. A., Winck, G. R., Weber, M. M., Nichols, E., & Sinervo, B. (2019). Impacts of forestation and deforestation on local temperature across the globe. *PLoS One*, *14*(3), e0213368. https://doi.org/10.1371/journal.pone.0213368

Ramankutty, N., & Foley, J. A. (1999). Estimating historical changes in global land cover: Croplands from 1700 to 1992. *Global Biogeochemical Cycles*, *13*(4), 997–1027. https://doi.org/10.1029/1999GB900046

Rigden, A. J., & Li, D. (2017). Attribution of surface temperature anomalies induced by land use and land cover changes. *Geophysical Research Letters*, *44*(13), 6814–6822. https://doi.org/10.1002/2017GL073811

Schneider, A., Friedl, M. A., & Potere, D. (2009). A new map of global urban extent from MODIS satellite data. *Environmental Research Letters*, *4*, 044003. https://doi.org/10.1088/1748-9326/4/4/044003

Schultz, N. M., Lee, X., Lawrence, P. J., Lawrence, D. M., & Zhao, L. (2016). Assessing the use of subgrid land model output to study impacts of land cover change. *Journal of Geophysical Research: Atmospheres*, *121*(11), 6133–6147. https://doi.org/10.1002/2016JD025094

Verbiest, W. W. M., Smith, G. R., Mirzagholi, L., Lauber, T., Zohner, C. M., Maynard, D. S., et al. (2023). Enhanced local cooling effects of forests across the globe. https://doi.org/10.1101/2023.10.17.562656

Winckler, J., Lejeune, Q., Reick, C. H., & Pongratz, J. (2019). Nonlocal effects dominate the global mean surface temperature response to the biogeophysical effects of deforestation. *Geophysical Research Letters*, *46*(2), 745–755. https://doi.org/10.1029/2018GL080211

Winckler, J., Reick, C. H., Luyssaert, S., Cescatti, A., Stoy, P. C., Lejeune, Q., et al. (2019). Different response of surface temperature and air temperature to deforestation in climate models. *Earth System Dynamics*, *10*(3), 473–484. https://doi.org/10.5194/esd-10-473-2019

Winckler, J., Reick, C. H., & Pongratz, J. (2017a). Robust identification of local biogeophysical effects of land-cover change in a global climate model. *Journal of Climate*, *30*(3), 1159–1176. https://doi.org/10.1175/jcli-d-16-0067.1

Winckler, J., Reick, C. H., & Pongratz, J. (2017b). Why does the locally induced temperature response to land cover change differ across scenarios? *Geophysical Research Letters*, *44*(8), 3833–3840. https://doi.org/10.1002/2017gl072519

Yuan, K., Zhu, Q., Zheng, S., Zhao, L., Chen, M., Riley, W. J., et al. (2021). Deforestation reshapes land-surface energy-flux partitioning. *Environmental Research Letters*, *16*(2), 024014. https://doi.org/10.1088/1748-9326/abd8f9

Zeng, Z., Piao, S., Li, L. Z. X., Zhou, L., Ciais, P., Wang, T., et al. (2017). Climate mitigation from vegetation biophysical feedbacks during the past three decades. *Nature Climate Change*, *7*(6), 432–436. https://doi.org/10.1038/nclimate3299

Zhang, M., Lee, X., Yu, G., Han, S., Wang, H., Yan, J., et al. (2014). Response of surface air temperature to small-scale land clearing across latitudes. *Environmental Research Letters*, *9*(3), 034002. https://doi.org/10.1088/1748-9326/9/3/034002

Zhao, Z., & Li, Y. (2026). Code and dataset for paper "Intercomparison of methods for disentangling local and nonlocal biophysical effects of land cover changes.". *Figshare*. [Dataset]. https://doi.org/10.6084/m9.figshare.30519305